Electronic structure of Al-Pd-Mn crystalline and quasicrystalline alloys

2002 J. Phys.: Condens. Matter 14 87

(http://iopscience.iop.org/0953-8984/14/1/308)

INSTITUTE OF PHYSICS PUBLISHING JOURNAL OF PHYSICS: CONDENSED MATTER

J. Phys.: Condens. Matter **14** (2002) 87–102 PII: S0953-8984(02)24139-9

Electronic structure of Al–Pd–Mn crystalline and quasicrystalline alloys

Vincent Fournee[1,7], Esther Belin-Ferre[1,8], Pierre Pecheur[2], Janusz Tobola[3], Zoltan Dankhazi[4], Anne Sadoc[5] and Herbert Müller[6]

[1] Laboratoire de Chimie Physique Matière et Rayonnement, UMR CNRS 7614, 11 rue Pierre et Marie Curie, 75231 Paris Cedex 05, France
[2] Laboratoire de Physique des Matériaux, UMR CNRS 7556, Ecole des Mines de Nancy, Parc de Saurupt, 54042 Nancy Cedex, France
[3] Faculty of Physics and Nuclear Techniques, Academy of Mining and Metallurgy, Alea Mickiewicza 30, 30-059 Krakow, Poland
[4] Institute for Solid State Physics, ELTE, Pasmany P. Setany 1/A, 1117 Budapest, Hungary
[5] LPMS, Université de Cergy-Pontoise, 95031 Cergy-Pontoise Cedex and LURE, 91405 Orsay Cedex, France
[6] Institüt für Experimentalphysik, TU-Wien, Wiedner Hauptstrasse 8-10, 1040 Wien, Austria

E-mail: belin@ccr. jussieu. fr

Received 20 April 2001, in final form 18 September 2001
Published 7 December 2001
Online at stacks.iop.org/JPhysCM/14/87

Abstract

An experimental and theoretical analysis of the electronic structure of Al–Pd alloys is presented. The experimental study, based on soft x-ray emission and absorption spectroscopies, is further extended to the case of quasicrystalline Al–Pd–Mn alloys and their approximants. The electronic structure is dominated by the sp–d hybridization. The Al-sp band is strongly modified by the interaction with the Pd-d states in the middle of the valence band. Close to the Fermi level, hybridization with the Mn-d states is found to enhance the structure induced pseudo-gap in the Al partial density of states, both in the icosahedral and the decagonal quasicrystalline phases.

1. Introduction

The electronic structure of quasicrystals (QCs), discovered by Shechtman *et al* in 1984, plays an important role in stabilizing these quasiperiodic structures. A Hume–Rothery type stabilization mechanism is indeed well established for icosahedral Al-based QCs. This is based on both theoretical predictions and experimental observations of a structure induced pseudogap in the electronic density of states (DOS) located at the Fermi level (E_F).

[7] Present address: 331 Spedding Hall, Ames Laboratory, Iowa State University, Ames, IA 50011, USA.
[8] Corresponding author.

In the Al–Cu–Fe icosahedral phase (i phase) for example, the pseudo-gap at E_F was observed by ultra-high energy resolution photoemission spectroscopy measurements (Stadnik *et al* 1997). A detailed analysis of the electronic structure of the i phase, compared to that of approximant phases and crystalline alloys with close chemical compositions has also been reported by us, based on x-ray emission and absorption spectroscopies (XES and XAS respectively) (Belin-Ferré and Dubois 1996 and references therein, Belin-Ferré *et al* 2000). A reduced intensity consistent with the presence a pseudo-gap at E_F was observed in the Al partial DOS, both in the i phase and in its approximants. These experiments were further extended to a set of Al–Cu alloys of the Hume–Rothery type and by cross-analysis, it was possible to show the importance of the hybridization between Al-sp states and transition metal (TM) d states at E_F, enhancing the scattering of the Fermi electrons (Fournée *et al* 1998).

In this article, we will describe the electronic structure of several Al–Pd and Al–Pd–Mn alloys, as a function of their chemical composition and atomic structure. We will point out similarities between the electronic structure of the Al–Pd–Mn and the Al–Cu–Fe i phases, which were expected based on their closely related atomic and electronic structures (Gratias *et al* 2000, Berger 1994). However, the Al–Pd–Mn quasicrystalline system is very unique, as it contains both a stable i phase and a stable decagonal phase (d phase), together with several identified approximant crystals. While i QCs are quasiperiodic in all three dimensions, d QCs are quasiperiodic only in the plane perpendicularly to its non-crystallographic axis and periodic along it. It follows that the physical properties of d QCs are characterized by a strong anisotropy and it was suggested that the pseudo-gap in the DOS would be destroyed by the remaining one-dimensional periodicity (Sabiryanov and Bose 1994). We will show here that the physical mechanisms responsible for the opening of the pseudo-gap in the i QCs are also observed in the d phase, at least in the partial Al DOS.

The valence and conduction bands (VB and CB respectively) have been measured by XES and XAS respectively. We also present DOS calculations performed using either the KKR or APW methods for the crystalline Al–Pd phases. These calculations are helpful in the interpretation of the experimental spectra and allow to distinguish those experimental features that could be due to many-body effects. In addition, the general trends deduced from the analysis on crystalline phases will be useful for further discussion of the electronic structure of Al–Pd–Mn quasiperiodic alloys. Indeed, although calculations are available for models of approximant crystals, experimental investigation of the electronic structure is still of particular interest since calculations are not possible for true Al–Pd–Mn QCs. It was also found that the details of the atomic structure model used can have a quite large influence on the resulting calculated DOS (Krajci 2000).

The paper is organized as follows. The samples used in this study are described in part 2. Three binary Al–Pd crystals and four ternary Al–Pd–Mn were investigated (namely i-$Al_{71}Pd_{19}Mn_{10}$, d-$Al_{69.8}Pd_{21}Mn_{18.1}$ and the orthorhombic approximants ξ'-$Al_{74}Pd_{21.6}Mn_{4.4}$ and T-$Al_{71}Pd_4Mn_{25}$). The experimental techniques and the calculation methods are briefly described in parts 3 and 4. The results are discussed in part 5 and a summary is presented in part 6.

2. Atomic structure

The data referring to the atomic structure of the various samples are collected in table 1. AlPd is a high-temperature cubic phase with the CsCl structure type (B2). Its space group is $Pm3m$ and the lattice parameter is $a = 0.3036$ nm. Hexagonal Al_3Pd_2 is of the λ-Al_3Ni_2 type with space group $P\bar{3}m1$ and lattice parameters $a = 0.4208$ nm and $c = 0.5150$ nm. A structural relationship between the CsCl and Al_3Ni_2 structure types and that of QCs was pointed out by

Table 1. Structure and composition of the Al–Pd–(Mn) alloys.

Sample	Structure and lattice parameters (nm)	Electron/ atom ratio (e/a)
AlPd	Cubic, CsCl type $Pm3m$, $a = 0.3036$	1.5
Al_3Pd_2	Hexagonal, $P\bar{3}m1$ λ-Al_3Ni_2 type, $a = 0.4208$ $c = 0.515$	1.8
Al_3Pd	Orthorhombic, $Pna2_1$ $a = 2.336$ $b = 1.6566$ $c = 1.232$	2.25
ξ'-$Al_{74}Pd_{21.6}Mn_{4.4}$	Orthorhombic, $a = 2.032$ $b = 1.650$ $c = 1.476$	2.09
T-$Al_{71}Pd_4Mn_{25}$	Orthorhombic, $Pnma$, $a = 1.476$ $b = 1.243$ $c = 1.256$	1.43
d-$Al_{69.8}Pd_{12.1}Mn_{18.1}$	Decagonal, period: 1.24	1.59
i-$Al_{71}Pd_{19}Mn_{10}$	Icosahedral	1.85

Dong (1996, 1995). Interest for these two compounds is motivated by the experimental fact that they usually appear as extra phases during crystal growth processing of i-Al–Pd–Mn QCs (Delaney *et al* 1997).

Al_3Pd is an orthorhombic crystal (Matsuo and Hiraga 1994). Its space group is $Pn2_1a$ and the lattice parameters are $a = 2.336$ nm, $b = 1.6566$ nm and $c = 1.232$ nm. It consists of flat and puckered layers exhibiting local pentagonal symmetry, stacked perpendicularly to the b axis. It is described as an approximant structure of a metastable decagonal Al–Pd–Mn quasicrystal, with a 1.6 nm periodicity along the b axis perpendicular to the quasiperiodic planes (Hiraga *et al* 1994).

The atomic structure of the ξ'-$Al_{74}Pd_{21.6}Mn_{4.4}$ approximant is nearly isomorphic to that of Al_3Pd, in particular the lattice parameters are almost equal as outlined by Boudard *et al* (1996). The T-$Al_{71}Pd_4Mn_{25}$ crystal is another orthorhombic approximant but differs from the ξ' and Al_3Pd ones by its chemical composition which is Mn rich. Its b cell parameter is 1.243 nm, similar to the periodicity of the stable d-$Al_{69.8}Pd_{12.1}Mn_{18.1}$ phase. pseudo-Mackay clusters (PMC) and Bergman clusters (BC) have been identified as the building units of these approximant structures (Behara *et al* 1998). The PMCs have chemically ordered shells whereas the BCs are chemically disordered. Most of the atoms in the Al_3Pd and ξ' approximants are described by PMCs whereas atomic positions in the T phase are mainly described by BC.

The structure of the decagonal quasicrystal can be described as a periodic stacking along the b axis of quasiperiodic layers, the periodicity being equal to 1.24 nm. Alternatively, the structure can be viewed as the packing of columnar clusters with fivefold symmetry and a diameter of $\approx$2 nm.

3. Experimental techniques

The electronic distributions of the VB and CB states were analysed using soft x-ray emission and absorption spectroscopies (XES and XAS). The principles of these spectroscopies have been summarized elsewhere (see, for example, Bonnelle (1987), Agarwal (1979)). The main advantage of the XES/XAS techniques over the most commonly used photoemission spectroscopies (PES) relies on their direct chemical and angular momentum selectivities, since it involves transition to a core hole localized on a particular ionized atom. To be more precise, XES and XAS probes the local DOS of the VB and CB averaged over the sites of each constituent element separately and, because dipole selection rules apply, the x-ray emission process is also symmetry selective. In the following, all the partial electronic distributions (listed in table 2) are adjusted in the binding energy (BE) scale where the Fermi level is the origin to allow for a meaningful discussion of the electronic structure. This can be achieved by measuring the BE of the core levels involved in each x-ray transition from independent

Table 2. Analysed x-ray transitions, probed states and energy range, analyser used, resolution and width of the inner level involved in the x-ray transitions.

X-ray transition	Symmetry of the probed states	Probed energy range (eV)	Width of inner level (eV)	Crystal or grating	Energy resolution of spectrometer (eV)
Al Kβ 3p→1s	VB Al 3p	1545–1565	<0.1	$SiO_2 10\bar{1}0$	0.2
Al $L_{2,3}$ 3s, d→$2p_{3/2}$	VB Al 3s, d	55–77	0.42	grating	0.3
Al K 1s→p	CB Al p	1555–1580	<0.1	$SiO_2 10\bar{1}0$	0.2
Pd L$\beta_{2,15}$ 4d–5s →$2p_{3/2}$	VB Pd 4d–5s	3145–3195	2.2	Beryl $10\bar{1}0$	0.3
Pd L_{III} $2p_{3/2}$ →d, s	CB Pd d–s	3160–3210	2.2	Si 111	0.3
Mn Lα 3d–4s →$2p_{3/2}$	VB 3d–4s	630–645	0.5	RbAP 111	

PES measurements (Belin and Traverse 1991). This adjustment procedure is valid only in the framework of the Koopman's theorem, which is based on the frozen orbital approximation (Agarwal 1979). However, beyond this approximation, we need to consider relaxation effects of the electronic levels in response to the presence of electron vacancies. We note that the final state of the photoemission process and the initial state of the x-ray transition are the same and both contain a core hole. But the initial state in PES is the ground state whereas the final state in XES contains a hole in the valence band. Therefore, while adjusting the partial DOS in the BE scale, we neglect the relaxation of the electronic levels due to the hole in the valence band. In the following, the comparison between experimental and theoretical positions of the partial DOS will show the validity of this approximation.

The XES measurements were carried out with Johann-type vacuum spectrometers. These were fitted with either a grating bent with a radius of 2 m or with crystals bent with a radius of 0.5 m. The XAS measurements were performed at the synchrotron radiation facility of LURE (Orsay, France) at the SA 32 beam line. This was equipped with a two SiO_2 $10\bar{1}0$ crystals monochromator. Experimental details and calculated values for the final energy resolution are given in table 2 for each of the analysed transitions. Note that the lifetime broadening of the core levels is often the most important limitation to the resolution in these techniques (Krause and Oliver 1979).

The core levels BE were measured with a photoemission spectrometer fitted with an Al anode as the x-ray source operating in ultra-high vacuum. The value for the Al 1s core level BE cannot be obtained directly. It was deduced from the Al $2p_{3/2}$ BE and from the measurements of the Al Kα_1 x-ray lines ($2p_{3/2} \rightarrow 1s$ transition). Similarly, the BE of Pd $2p_{3/2}$ was deduced from the measurements of the Pd $3d_{5/2}$ BE and the Pd $3d_{5/2} \rightarrow 2p_{3/2}$ x-ray emission transition energy. Finally, we could locate E_F on the various transition energy scales within ± 0.2 eV for Al and ± 0.3 eV for the other elements.

Two methods of calculation

The calculations of the band structures of AlPd and Al_3Pd_2 were performed with the KKR method (Bansil *et al* 1992, Kaprzyk and Bansil 1990, Kaprzyk 1997), while the calculation for the Al_3Pd alloy was performed using the augmented plane wave (APW) method (Matheiss *et al* 1968). These two different methods were used because of the limited number of crystalline structure implemented within each program.

The self-consistent KKR calculations were performed using scalar relativistic terms within the muffin-tin approximation. The local spin density approximation was used with an exchange–correlation part of the Barth–Hedin form (von Barth and Hedin 1972). The same

muffin-tin radius was chosen for the two atoms. The results show both the total DOS and the muffin-tin contribution to the DOS. The similarity in shape of both curves indicates that the muffin-tin approximation is satisfactory for these compounds.

The DOS of a hypothetical in the Cu_3Au structure was calculated using the APW method (Matheiss *et al* 1968). The APW calculation was performed self-consistently using scalar relativistic terms within the muffin-tin approximation. Exchange and correlation of the electrons were treated within the local-density approximation using the formalism of Hedin and Lundqvist (1971). The equilibrium lattice parameters were determined by fitting the calculated total energy at various lattice constants with a least-squares fit (Birch 1978). The highest s, p and d orbitals were treated as VB levels, all other states being core levels.

For the icosahedral and decagonal compounds, we refer to band structure calculations carried out within the framework of the tight binding-linearized muffin-tin orbital (TB-LMTO) method on model approximants of the icosahedral and decagonal structures of nominal compositions $Al_{70.7}Pd_{20.6}Mn_{8.6}$ and $Al_{70}Pd_{13}Mn_{17}$, respectively (Krajci *et al* 1995 and 1997). Partial DOS for non topological equivalent atoms were calculated using a recursion method.

For a meaningful comparison between theoretical DOS and experimental spectra, the calculated partial DOS were convoluted with the Lorentzian distribution function of the core level involved in the x-ray transition and by a Gaussian function to account for the instrumental broadening of the spectrometer. We did not calculate the matrix element of the dipolar transition between the VB states and the core states assuming that it is a smooth function of the energy over the width of a band (McCaffrey and Papaconstantopoulos 1974). For the Al $L_{2,3}$ spectra, we added the s DOS with two-fifths of the d DOS, following the prescription of Goodings and Harris (1969). As no absolute values of the DOS can be derived from the XES technique, all the calculated spectra are normalized to their maximum intensity.

4. Results and discussion

1-valence states

The VB of the Al–Pd alloys are mainly formed by the Pd-4d, and the Al 3s, 3p and 3d-like states whereas for the Al–Pd–Mn alloys, Mn-3d states are also involved. The Pd-4d and Mn-3d states represent the main contribution to the VB due to their high density of levels (Zhang *et al* 1994, Krajci *et al* 1995, 1997). However, these states are more localized and thus less sensitive to their chemical environment than the more extended Al states with s and p character. It is therefore of importance to analyse the distributions of the Al states and their modifications as a function of the chemical ordering and composition.

The experimentally derived VB are presented in figure 1(a) for the three crystalline Al–Pd alloys and in figure 1(b) for the four Al–Pd–Mn alloys. As no absolute values of the DOS can be derived from the XES technique, all the spectra are normalized to their maximum intensity after a proper background substraction and are presented in arbitrary units. The calculated DOS for the three crystalline Al–Pd alloys are presented in figure 2, and the corresponding calculated spectra are shown in figure 3.

a-Pd-4d states

The Pd $L\beta_{2,15}$ spectra (4d, 5s $\rightarrow$ $2p_{3/2}$ transitions) mainly reflect the distribution of the occupied Pd-4d states. This is due to the x-ray transition matrix elements that largely favour transitions from d levels rather than from s levels. Furthermore, the calculated Pd-5s DOS are so low in the alloys that we can ignore their contribution to the experimental spectra. In all samples, the

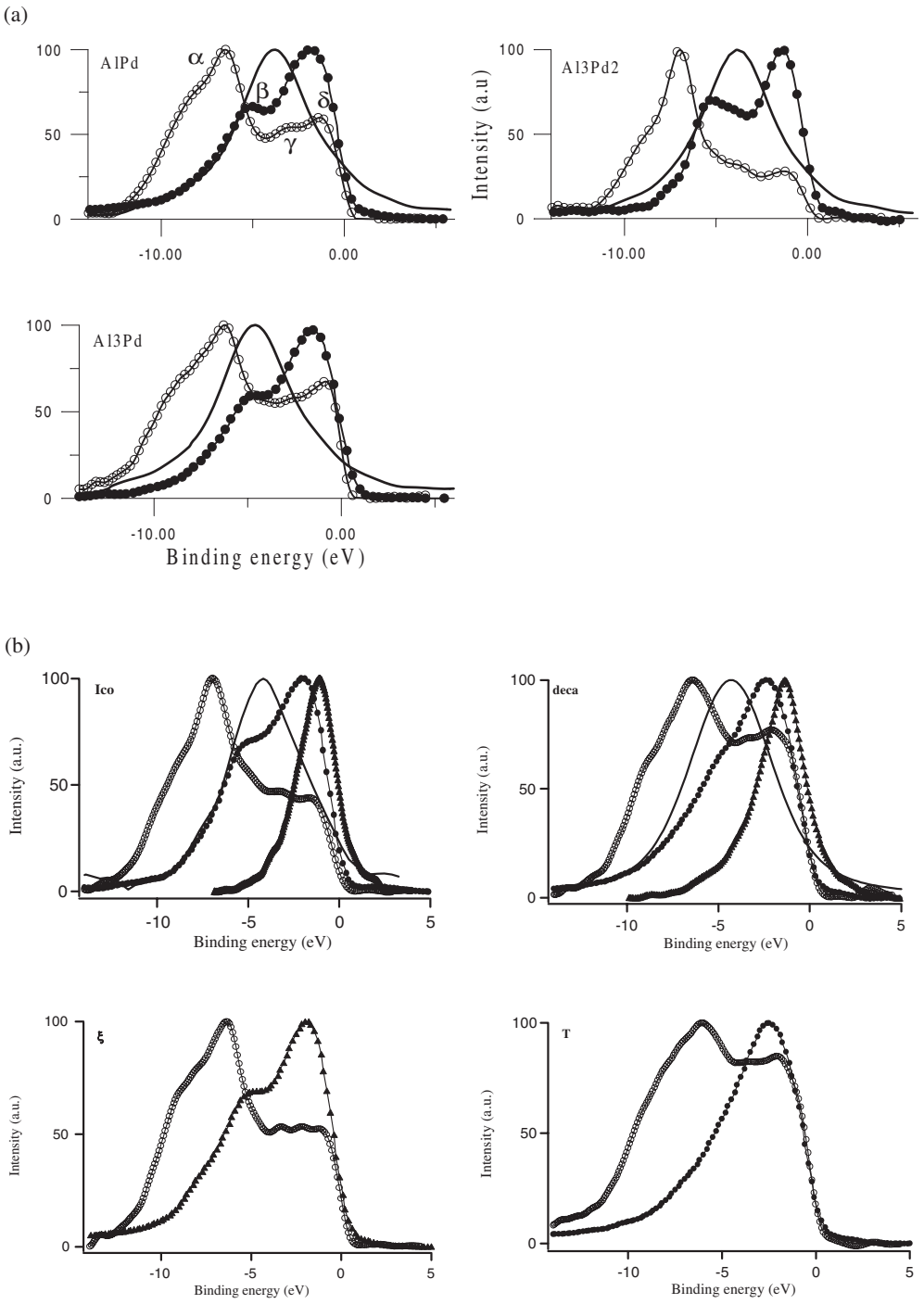

Figure 1. (a) Experimental Al-3s, d (Al $L_{2,3}$ spectra, open dots), Al-3p (Al Kβ spectra, solid dots) and Pd-4d (Pd L$\beta_{2,15}$, solid curve) distribution curves in AlPd, Al_3Pd_2 and Al_3Pd crystalline compounds. (b) Experimental Al-3s, d (Al $L_{2,3}$ spectra, open dots), Al-3p (Al Kβ spectra, solid dots), Pd-4d (Pd L$\beta_{2,15}$ spectra, solid curve) and Mn-3d (Mn Lα spectra, triangles) distribution curves in i-$Al_{71}Pd_{19}Mn_{10}$, d-$Al_{69.8}Pd_{21}Mn_{18.1}$, ξ'-$Al_{74}Pd_{21.6}Mn_{4.4}$ and T-$Al_{71}Pd_4Mn_{25}$.

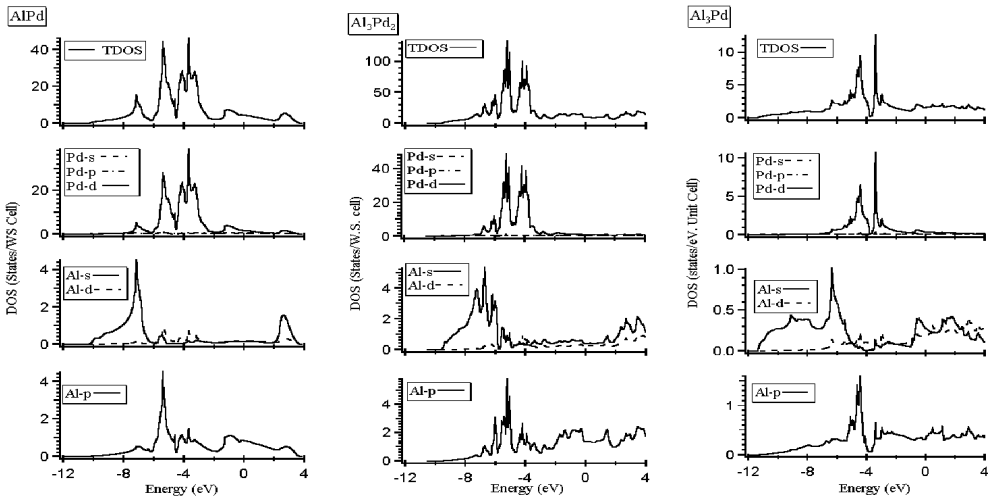

Figure 2. Calculated total and partial densities of states of AlPd (left column), Al_3Pd_2 (middle column) and Al_3Pd in the Cu_3Au structure (right column).

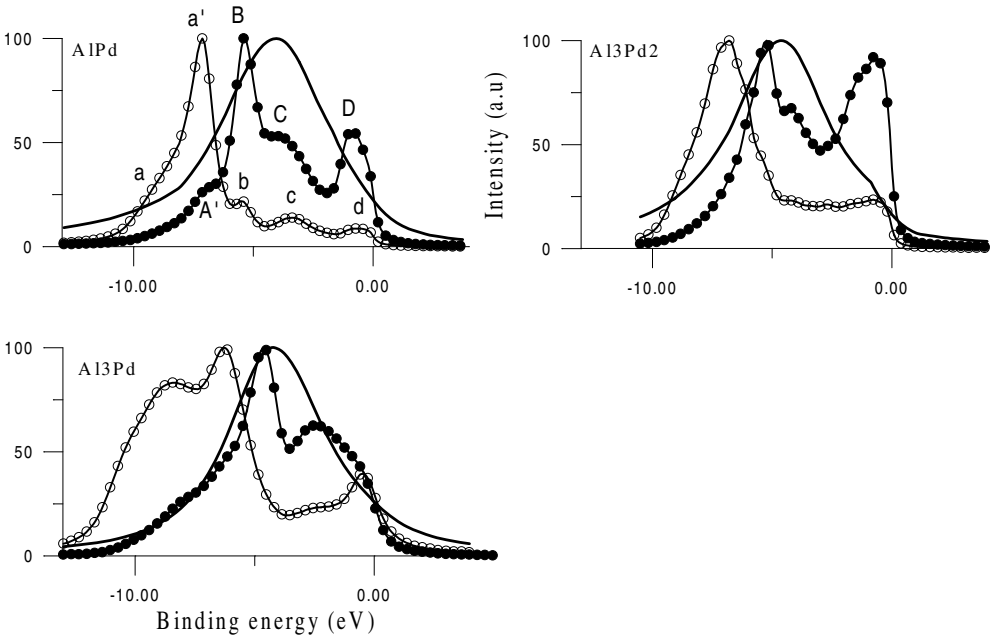

Figure 3. Calculated (see text) Al-3s, d (open dots), Al-3p (solid dots) and Pd-4d (solid curve) distribution curves in AlPd, Al_3Pd_2 and Al_3Pd crystalline compounds.

Pd-4d states form a broad band located at about 4 eV below E_F (figures 1 and 3), which is structureless due to the large lifetime broadening of the $2p_{3/2}$ core-level.

In pure Pd, the d-band lies at a BE of 2.1 eV and there is still a high DOS at E_F. The situation is different in all of the alloys, where the d-band is shifted toward higher BE. The measured and calculated shifts are as large as about 2.0 eV and they slightly increase as the Pd

concentration decreases. The experimental and calculated values of the Pd-4d peak maximum BE are listed in table 3 when available. The chemical shifts of the Pd-3d core levels measured by PES are of the same order of magnitude as the shifts of the Pd-4d bands. Small discrepancies are found between the calculated and experimental positions. The observed differences may be attributed to effects not taken into account in the calculations due to either the creation of the core hole on the remaining electronic cloud or to matrix elements. Nevertheless, the large shift observed is consistent with the filling of the Pd-4d band upon alloying with Al. As a consequence, there is a decrease of the corresponding partial DOS at E_F in the alloys as compared to pure Pd. The filling of the Pd-4d band should not be considered as a result of a real charge transfer from electropositive Al to Pd atoms but rather, as we will show in the following, the Pd-4d bands become filled by hybridization effects. An important issue is that there is always some d character at E_F. We will return to this point later.

b-Mn-3d states

The Mn Lα spectra (3d, 4s $\rightarrow$ $2p_{3/2}$ transitions) mainly reflect the distribution of the occupied Mn-3d states, for the same reasons as already explained in the case of the Pd L$\beta_{2,15}$ spectra. The Mn-3d states form a band located at a BE of 1.0 and 1.3 eV in the i and d phases respectively (figure 1(b)). These positions are in excellent agreement with the positions calculated by Krajci *et al* for model approximants of the i and d phases (Krajci *et al* 1995 and 1997). The full-width at half-maximum of the Mn-d band is 2.5 and 3 eV in the i and d phases respectively, much smaller than the Pd-d band. This is partly due to the core-level lifetime broadening which is not so severe in the case of Mn (see table 2). As compared to the Mn metal, the bandwidth is also smaller in the Al–Pd–Mn alloys.

Band narrowing in the alloys is a consequence of the decrease in the d–d hopping amplitudes and of the number of hopping channels. In a simple tight-binding picture, the band width grows with the number Z of nearest neighbours as $Z^{1/2}$ and with enhanced overlap between the wave functions localized on adjacent atomic sites. In the case of the i phase, the average coordination numbers N_c have been deduced from EXAFS measurements (Sadoc and Dubois 1993). Mn atoms have on average eight nearest-neighbours (seven Al atoms and one Pd located at 2.5 and 2.75 Å respectively), whereas N_c vary from 12–16 in the pure metal, with interatomic distances ranging from 2.25–3 Å. This is consistent with a narrowing of the Mn-3d band in the i phase.

c-Al bands

The experimental Al-3s, d and Al-3p occupied bands for all the alloys and for pure Al-fcc are compared in figure 4. In the pure metal, the bands have parabolic shapes typical of a free-electron metal. This has been described thoroughly in the past (Rooke1968a, 1968b, 1968, 1974, Neddermeyer 1974). A sharp narrow peak near E_F can be seen in the Al-3s, d band, which is mainly due to a many-body effect (the infra-red catastrophe). It arises from low-energy electron–hole pairs created simultaneously to the formation of the core-hole and is typical of metallic systems (Nozières and de Dominicis 1969). This is the counterpart in XES of the well known tailing effect of core level line shapes of metals in XPS (Mahan 1967). From figure 4, clearly, the electronic distributions of Al in the Al–Pd (Mn) alloys are no longer smooth functions of energy. They are strongly modified by the interaction with the more localized Pd-4d states in the middle of the valence band and within about 1 eV below E_F with Mn-3d states in the Al–Pd–Mn alloys. Common features for all these samples can be outlined as follows.

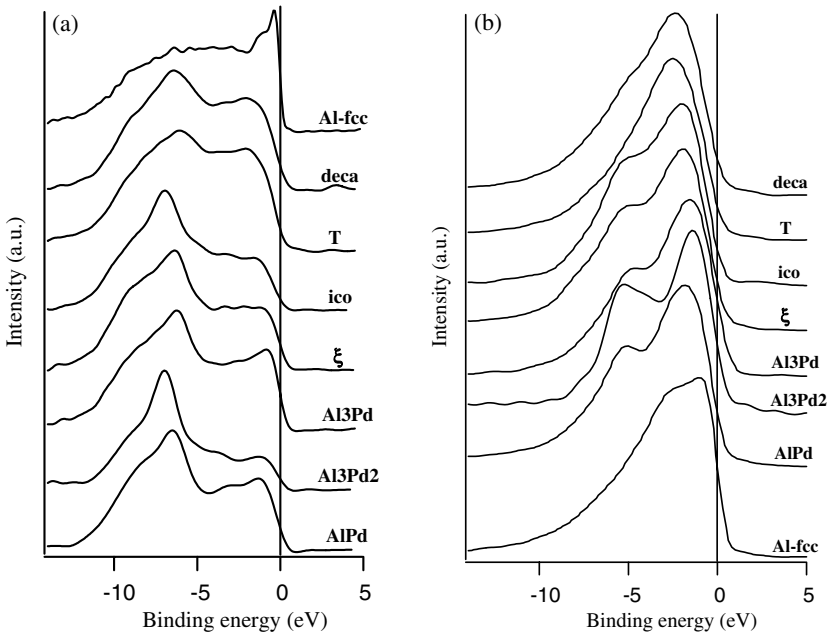

Figure 4. (a) Experimental Al-3s, d distribution curves (Al $L_{2,3}$ spectra) in Al-fcc and in Al–Pd(–Mn) alloys. (b) Experimental Al-3p distribution curves (Al Kβ spectra) in Al-fcc and in Al–Pd(–Mn) alloys.

The density of Al-3s, d states is enhanced at high BE and strongly suppressed in the energy range of the Pd-4d band. The Al-3p bands are split into two parts located on each side of the Pd-4d states. The deformation of the Al sub-band can be interpreted as the effect of the coupling between a broad band of extended states and a localized d band (Belin *et al* 1992). Such an interaction has been described theoretically by Terakura (1977) in terms of a Fano-like effect resulting from the mutual repulsion between sp and d states. As a consequence, Al-3s and 3p electrons form bonding and anti-bonding states located on each side of a dip at the anti-resonance position, whose energy corresponds to the top of the Pd-4d band. This behaviour is very similar to the Fano effect, well known in Raman spectroscopy.

In the case of crystalline Al–Pd samples, the experimental Al $L_{2,3}$ spectra (Al-3s, d states) show significant plateaus in the region 0–5 eV (figure 4(a)), as compared to the calculated ones seen in figure 3. The origin of this discrepancy can be two-fold. First, we have neglected the variations in the matrix element of the transition, which may lead to an overestimation of the intensity in the high BE side of the calculated spectra. Second, cross-transitions to the Pd d states and Al d states can also occur, leading to a more intense experimental signal in the energy range where these states overlap, i.e. in the region 0–5 eV. In Al–Pd–Mn alloys, cross-transitions to the Mn d states and Al d states can also occur. This results in a further increase of the experimental intensity in the 0–5 eV BE energy range with increasing Mn content. For higher BE, these effects are not very important and the intensity is attributed to Al s states. We note that the structures of the spectra are much broader than those from the calculation. This is somewhat surprising, as the effect of instrumental and core-level lifetime broadening have been taken into account in the calculated spectra. A possible explanation of the observed discrepancies could be the lifetime broadening related to the hole in the valence band (final state effect), which can be large in some cases are in some cases (Liebsch 1981),

Table 3. Experimental and calculated binding energies of the maximum of the Pd-d and Al-s bands in Al–Pd(–Mn) alloys (all values in eV). The number Δ refers to the positions of the maximum Al-3p distribution curve and $I(E_F)$ refers to its intensity at E_F, expressed in % of its maximum.

Compound	Expt. Pd-d	Theor. Pd-d	Exp. Al-s	Theor. Al-s	Δ	$I(E_F)$ %
Al					1.1	50
Pd	2.1 ± 0.2					
AlPd	3.8 ± 0.2	4.0	6.5 ± 0.2	7.0	1.8	29
Al_3Pd_2	4.0 ± 0.2	4.6	7.0 ± 0.2	6.8	1.4	36
Al_3Pd	4.4 ± 0.2	4.2	6.2 ± 0.2	6.3	1.6	43
i-Al–Pd–Mn	4.2 ± 0.2	4.0	6.9 ± 0.2	6.8	2.1	19
ξ'-Al–Pd–Mn	4.2 ± 0.2	NA	6.5 ± 0.2	NA	2.0	27
d-Al–Pd–Mn	4.3 ± 0.2	4.1	6.4 ± 0.2	6.1	2.4	19
T-Al–Pd–Mn	NA	NA	6.5 ± 0.2	NA	2.5	19

and that is not taken into account in the calculated spectra. However, the overall agreement between experimental and calculated distributions is fairly good since the main features of the experimental and the calculated Al-s and Al-d curves are at same BE. See for example the experimental and calculated curves for AlPd. The features labelled as α, α' β, γ and δ on the experimental curves (figure1(a)) are at same BE than peaks noted as A′, B, C, D and a, a′, b, c and d on the calculated curves (figure 3). The same holds true for Al_3Pd_2 and Al_3Pd.

The maximum peak intensity of the experimental and calculated Al-3s, d bands are listed in table 3. In the model proposed by Terakura, the position of the s-band maximum is strongly connected to the anti-resonance position and the distance between them depends on the coupling between the Al-sp and Pd-d states. This, in turn, should be sensitive to the local atomic environment. This is clearly shown on figure 5, where we have plotted the calculated Al-s DOS projected onto the two different types of Al sites in Al_3Pd_2. The Al-1 type of site has six Pd nearest-neighbours located at 2.55 Å whereas the Al-2 type of site has only four Pd nearest-neighbours, at about the same distance. This results in a higher coupling of the Al-s states with the Pd-d states and accordingly, a larger shift of the corresponding DOS is observed.

In the Al-p sub-bands, we also found that the contribution to the intensity of the high BE side of the VB seems to be overestimated in the calculation (see figures 1(a) and 3). A possible explanation could be that the variation in the matrix element of the transition is not the smooth function of the energy that we have assumed and, therefore, should be taken into account to obtain a better agreement. Apart from this difficulty in the relative intensities, the splitting of Al-p states in the bonding and antibonding peaks located on both sides of the Pd-d band is confirmed by the calculations. We note also that the intensity of the bonding peak (at -5 eV) strongly depends on the Pd content.

Close to the Fermi level, the maximum of the Al-3p distribution is systematically shifted towards the high BE as compared to pure Al (figure 4(b) and table 3). In the pure metal, the maximum peak intensity is located at $\Delta = -1.1$ eV and the intensity of the distribution at E_F, denoted as $I(E_F)$, is 50% of its maximum. In the Al–Pd alloys, Δ is -1.8, -1.4 and -1.6 eV and $I(E_F)$ is 29, 36 and 36% for AlPd, Al_3Pd_2 and Al_3Pd respectively. The Δ values are larger in the ternary Al–Pd–Mn compounds, where they vary from -2.1 to -2.5 eV (figure 4(b)). Δ increases with the Mn concentration, which is the result of stronger sp–d hybridization between Al and Mn states. It follows that $I(E_F)$ is lowered to about 19% in all the ternary alloys. The ξ'-approximant is an exception to that ($I(E_F) = 27\%$), due to the low Mn content in this phase. As already mentioned, the intensity at E_F of the Al-3s, d distribution is also reduced in all these alloys as compared to the Al–Pd samples. Therefore, these experimental

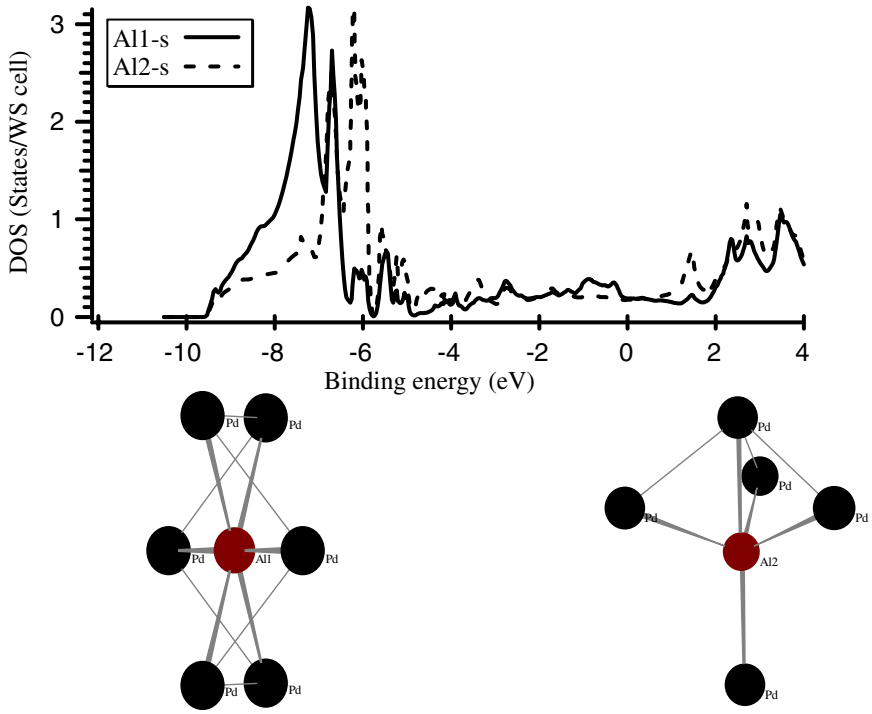

Figure 5. Top: Al-s DOS for Al-1 site (0, 0, 0) and Al-2 site ((1/3, 2/3, z) with $z = 0.648$) in Al_3Pd_2 collected in the Wigner–Seitz cell. Bottom: Pd atoms (in black) surrounding the Al atoms (in red). The bottom left structure represents Al-1 sites, and the bottom right the Al-2 sites.

(This figure is in colour only in the electronic version)

results are consistent with the presence of a pronounced pseudo-gap at E_F in the Al partial DOS of all these Al–Pd–Mn compounds, including the decagonal phase and its approximant.

QCs as well as their approximants usually satisfy the Hume–Rothery criteria. Indeed, their constituent elements have small differences in atomic radii and electronegativity and their electronic density is such that the Fermi electrons are strongly scattered by Bragg planes (Tsai 1997). This effect results in a depletion of the DOS located at the Fermi level and a minimization of the electronic contribution to the total energy of the system (Blandin 1967, Belin-Ferré *et al* 2000). The small reduction observed in $I(E_F)$ in the Al–Pd crystalline alloys as compared to the pure metal could be due to this kind of effect. Assuming that the simple free-electron model is valid in the present case, if we assume that the numbers of valence electrons are three and zero for Al and Pd, respectively, then the value of the Fermi wavevector k_F would be 1.461 Å^{-1} for AlPd and 1.495 Å^{-1} for Al_3Pd_2 (Janot 1997). From the calculated x-ray diffraction pattern of these well known structures, we derived the reciprocal lattice vector K_{hkl} corresponding to the most intense diffraction peaks and we found $K_{110}/2 = 1.455$ Å^{-1} for AlPd and $K_{012}/2 = 1.490$ Å^{-1} for Al_3Pd_2. For these two alloys, we should be in a situation of the Hume–Rothery type, where $k_F \sim K/2$. However, the DOS calculation does not show any pseudo-gap at E_F, although many structures due to the scattering of the valence electrons by Bragg planes can be seen on the Al partial DOS at energies $(hK)^2/8m$ from the bottom of the VB (figure 2).

The magnitude of the Fourier component $|V_K|$ of the potential seen by the electrons and the multiplicity of the corresponding Bragg planes determine the width and the depth of the pseudo-gap. The potential V_K can be written as the product

$$V_K = S(K) \cdot w(K) \tag{1}$$

where $S(K)$ is the structure factor and $w(K)$ is a form factor. The intensity of a Bragg peak in the x-ray diffraction pattern is determined by $S(K)$, but it is not straightforward that an intense Bragg peak necessarily leads to a strong potential V_K (Friedel 1988). In the case of the Al–Pd alloys discussed above, it is therefore possible that no pseudo-gap opens at E_F due to a weak ineffective potential V_K, despite of the strong diffraction peak at $K \sim 2k_F$. These results show that the application of the Hume–Rothery picture using the simple free-electron mentioned above is not valid for these Al–Pd alloys.

As noted in the introduction, Al_3Pd is an approximant phase of a metastable decagonal Al–Pd alloy. Whereas in d-AlPdMn we observed that the maximum of the Al-3p distribution is shifted towards high BE and its intensity at $E_F(I(E_F))$ is strongly suppressed as compared to pure Al, no such evidence has been found for the approximant phase Al_3Pd. Here, only a slight decrease is observed, of the same order as that found in AlPd and Al_3Pd_2. Consequently we cannot assess the existence of a pseudo-gap for the Al_3Pd approximant phase.

We mentioned above that, in Al–Pd–Mn compounds, a strong hybridization between the Al states and the Mn-3d states is present close to E_F (see also Belin *et al* (1991), (1994)). Previous theoretical studies on Al-transition metal alloys of the Hume–Rothery type have shown that the effect of the sp–d hybridization at E_F leads to an increase of the potential diffracting the Fermi electrons (Trambly de Laissardière *et al* 1995). This results in a larger pseudo-gap, that is more easily observable within our experimental resolution.

Two conduction states

a-Pd L_{III} photoabsorption edge. The Pd L_{III} absorption spectra are presented in figure 6 in the x-ray transition energy scale. In the pure metal, the spectra is characterized by an intense peak (called 'white line') corresponding to electronic transitions from $2p_{3/2}$ levels towards the first unoccupied levels with d symmetries, just above E_F. The structures observed at 8 and 14 eV from the absorption edge in pure Pd are due to transitions toward d–s hybridized states (Sham 1985). In the alloys, the absorption edge is shifted by more than 2 eV toward the high transition energies. This shift represents the chemical shift (ΔE_b) of the Pd $2p_{3/2}$ core level measured by XAS and after complete relaxation of the electronic states in the presence of the core hole. Assuming that the chemical shift is the same for all the Pd core-levels, ΔE_b measured by XAS is slightly higher than ΔE_b by XPS. The difference expresses the fact that the final state of the absorption process (an electron in the conduction band) contribute to the screening of the core hole (Sham 1985).

The width of the absorption edge can be estimated from the distance between the peak maximum and the energy position of the inflection point. The width is found larger in the alloys (from 2.5 to 3.6 eV) than for Pd metal (1.9 eV). We also note that the structures due to d–s hybridized states are modified in the alloys. This indicates that a redistribution of the states has occurred in the CB.

For a given element, the intensity of the white line decreases when the d band is being filled. Pd has ~0.36 holes per atom in its d band (Vuillemin and Priestley 1965). The presence of a white line in the alloys show that they are still some unoccupied Pd-d levels just above E_F. This is confirmed by our calculations (figure 2), where a small amount of states with Pd-d character can be seen above the Fermi level. Such an observation may seem contradictory with

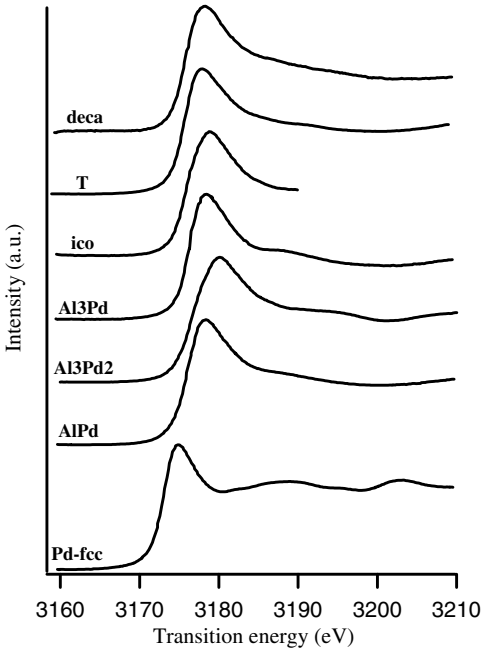

Figure 6. Pd L_{III} x-ray absorption spectra of Pd and Al–Pd(–Mn) alloys in the transition energy scale, normalized to their maximum intensity after subtraction of the proper background.

the filling of Pd-4d band previously noted. We infer that this gives evidence that the filling of the d band should not be interpreted as a charge transfer from the relatively electropositive Al to the Pd sites. It is more likely the result of the coupling between the Al-sp and Pd-d states that modifies the structure of the sp band and induces a complete redistribution of the electronic states in the valence and conduction bands. This point confirms experimentally the interpretation of the 'apparent negative valence' of the TM in Al–TM alloys proposed by Trambly *et al* (1993). Indeed, these authors emphasize that the negative valence of the TM does not correspond to a real charge transfer from Al towards unoccupied orbitals of the TM atoms. They propose that rather it arises from the increase of the number of Al-sp states below E_F, as compared to a free-electron band, due to sp–d hybridization. This is indeed in agreement with the results presented above.

b-Al K photoabsorption edge. The valence and conduction Al-3p and Al-p sub-bands are presented in figure 7 for Al-fcc and several Al–Pd–Mn phases. The intensities of each sub-band at E_F are adjusted using the following procedure. The Al-3p distribution measured by XES is normalized to the maximum of its intensity. Then, to normalize the intensity scale of the CB, we are forced to adjust the intensity of the Al-p CB measured by XAS at E_F to that of the Al-3p valence band, because the distribution of Al states with p symmetry should be continuous across E_F. This adjustment procedure reveals a strong asymmetry of the unoccupied Al-p band in the ternary alloys. The CB edge is less steep than the VB edge. Note however that for a given compound, the relative intensity of the CB strongly depends on the corresponding value of $I(E_F)$. The smaller $I(E_F)$ is, the more pronounced will be the asymmetry of the CB. This fact should be kept in mind when comparing the relative intensities of the CB in the various compounds.

The flattened CB is not quite well reproduced by band structure calculations performed on model approximants of the i and d phases. The corresponding calculated spectra, using the calculated partial Al p DOS of Krajci *et al* (Krajci 1995, 1997), are shown on figure 7.

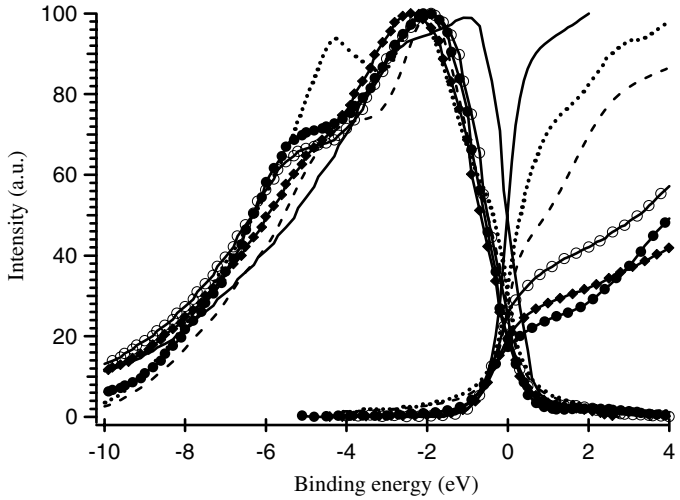

Figure 7. Experimental Al-p conduction bands (Al K spectra) in pure Al (solid curve), i-$Al_{71}Pd_{19}Mn_{10}$ (solid dots), d-$Al_{69.8}Pd_{21}Mn_{18.1}$ (diamond), ξ'-$Al_{74}Pd_{21.6}Mn_{4.4}$ (open dots) measured by XAS. Calculated Al-p conduction bands in 8/5-$Al_{70.7}Pd_{20.6}Mn_{8.6}$ and τ^2T-$Al_{70}Pd_{13}Mn_{17}$ model approximants of the i and d phase respectively (see Krajci *et al* (1995), (1997)). The left side of the plot shows the corresponding Al-3p valence bands.

The slope of the calculated CB edge is intermediate between that of Al-fcc and the Al–Pd–Mn compounds. It is not clear if such a flattened CB is real or is influenced mainly by the adjustment procedure we use and which makes the slope of the CB edge very sensitive to the exact location of E_F. A shift of 0.2 eV, which is our experimental uncertainty in locating E_F, could lead to a better agreement between experiment and theory. By taking account of this uncertainty, we verified however that a flattened CB is still observed in the QCs as compared to pure Al. Finally, we mention as a remark that the hierarchical cluster model proposed to described the i phase predicts an asymmetry of the DOS at E_F (Janot and de Boissieu 1994), in agreement with our observations.

5. Summary

We presented a detailed analysis of the electronic structure of various Al–Pd(–Mn) alloys as a function of their chemical compositions and atomic orders. It appears that the electronic structure of Al–Pd–Mn QCs, approximants and of the more simple Al–Pd crystals is dominated by the sp–d hybridization. In the middle of the VB, sp–d hybridization results in a filling of the Pd-4d band associated with strong modifications of the sp band. Band structure calculations for Al–Pd alloys show that the reshaping of the sp band is very sensitive to the details of the local atomic environments. The Pd L_{III} absorption spectra show that there is no real charge transfer from Al toward the vacant orbitals of Pd. This illustrate the concept of negative effective valence of transition metals introduced for Al–TM Hume–Rothery alloys (Raynor and Waldrom 1949, Friedel 1992, Trambly de Laissardière *et al* 1993).

Close to the Fermi level, a systematic shift of the Al VB edge toward higher binding energies is observed. The magnitude of the shift increases with the Mn concentration. A reduced intensity at E_F is measured, consistent with the presence of a pronounced pseudo-gap in the Al partial DOS of all these Al–Pd–Mn compounds. This conclusion also includes the

decagonal phase and its approximant and gives experimental support to the band structure calculation performed by Krajci *et al* for a model approximant d-$Al_{70}Pd_{13}Mn_{17}$ (Krajci *et al* 1997). The sp–d hybridization between Al sp and Mn d states is found to be an important factor in the formation of the pseudo-gap. In Hume–Rothery type alloys, its effect is to increase the magnitude of the potential diffracting the Fermi electrons (Trambly de Laissardière *et al* 1995, Fournée *et al* 1998). The location of the Fermi level in a minimum of the Al partial DOS, produced by Bragg scattering and enhanced by hybridization, should also contribute to the stability of the decagonal phase and its approximant.

Acknowledgments

We are pleased to thank A M Flanck, P Lagarde (LURE, France) for their assistance in experiments and D A Papaconstantopoulos (NRL, USA) for his collaboration in APW band structure calculations. We are grateful to M de Boissieu (Grenoble, France), M Erbudack and C Beeli (Zurich, Switzerland), Y Calvayrac (Vitry, France) and J M Dubois (Nancy, France) for providing us with high quality samples. We also thank Dr M Krajci (TU Wien and Bratislava) for communicating his DOS calculations. The hospitality offered to VF, ZD and EB-F by the Institute for Experimental Physics at the Technical University of Vienna (Austria) is warmly acknowledged. One of us (ZD) wish to acknowledge the Hungarian Academy of Sciences for financial support through the Bolyai János Research Fellowship. This work has been supported in part by the Austrian Ministry of Research, East–West Co-operation program under the title 'Soft x-ray spectroscopy of metallic systems'.

References

Agarwal B W 1979 *X-Ray Spectroscopy. An Introduction* (Berlin: Springer)
Bansil P, Kaprzyk S and Tobola J 1992 *Applications of Multiple Scattering Theory in Material Science* vol 252, ed W H Butler, P H Dederichs, A Gonis and R L Weaver (Pittsburg, PA: Materials Research Society) p 50
Behara L, Duneau M, Klein H and Audier M 1998 *Quasicrystals* ed S Takeuchi and T Fujiwara (Singapore: World Scientific) p 207
Belin E, Dankhazi Z, Sadoc A, Calvayrac Y, Klein T and Dubois J M 1992 *J. Phys.: Condens. Matter* **4** 4459
Belin E, Dankhazi Z, Sadoc A and Dubois J M 1994 *J. Phys.: Condens. Matter* **6** 8771
Belin E and Traverse A 1991 *J. Phys.: Condens. Matter* **3** 2157
Belin-Ferré E and Dubois J M 1996 *J. Phys.: Condens. Matter* **8** L717
Belin-Ferré E, Fournée V and Dubois J M 2000 *J. Phys.: Condens. Matter* **12** 8189
Berger C 1994 *Lectures on Quasicrystals* ed F Hippert and D Gratias (Paris: Les Editions de Physique) p 463 and references therein
Birch F 1978 *J. Geophys. Res.* **83** 1257
Blandin A 1967 *Phase Stability in Metals and Alloys* ed P S Rudman, J Stringer and R I Jaffee (New York: McGraw-Hill) p 115
Bonnelle C 1987 X-ray spectroscopy *Annual Report* C The Royal Society of Chemistry
Boudard M, Klein H, de Boissieu M and Audier M 1996 *Phil. Mag.* A **74** 939
Delaney D W, Bloomer T E and Lograsso T 1997 *New Horizons in Quasicrystals* ed A I Goldman, D J Sordelet, P A Thiel and J M Dubois (Singapore: World Scientific) p 45
Dong C 1995 *J. Phys. I France* **5** 1625
Dong C 1996 *Phil. Mag.* A **73** 1519
Fournée V, Esther Belin-Ferré E and Dubois J M 1998 *J. Phys.: Condens. Matter* **10** 4231
Friedel J 1988 *Helv. Phys. Acta* **61** 538
Friedel J 1992 *Phil. Mag.* B **65** 1125
Goodings D A and Harris R 1969 *J. Phys. C: Solid State Phys.* **2** 1808
Gratias D, Puyraimond F, Quiquandon M and Katz A 2000 *Phys. Rev.* B **63** 24 202
Hedin L and Lundqvist B I 1971 *J. Phys. C: Solid State Phys.* **4** 2064
Hiraga K, Abe E and Matsuo Y 1994 *Phil. Mag. Lett.* **70** 163

Janot C 1997 *J. Phys.: Condens. Matter* **9** 1493
Janot C and de Boissieu M 1994 *Phys. Rev. Lett.* **72** 1674
Kaprzyk S 1997 *Acta Phys. Pol.* A **91** 135
Kaprzyk S and Bansil P 1990 *Phys. Rev.* B **42** 7378
Krajci M, Hafner J and Mihalkovic M 1997a *Phys. Rev.* B **55** 84
Krajci M, Hafner J and Mihalkovic M 1997b *Phys. Rev.* B **62** 243
Krajci M, Windisch M, Hafner J, Kresse G and Mihalkovic M 1995 *Phys. Rev.* B **51** 17 355
Krause M O and Oliver J H 1979 *J. Phys. Chem. Ref. Data* **8** 329
Liebsch A 1981 *Phys. Rev.* B **23** 5203
Mahan G D 1967 *Phys. Rev.* **163** 612
Matheiss L F, Wood J H and Switendick A 1968 *Methods in Computational Physics* vol 8, ed A Adler, S Fernbach and R Rotenberg (New York: Academic)
Matsuo S and Hiraga K 1994 *Phil. Mag. Lett.* **70** 155
McCaffrey J W and Papaconstantopoulos D A 1974 *Solid State Commun.* **14** 1055
Neddermeyer H 1974 *Z. Phys.* **271** 329
Nozières P and de Dominicis C T 1969 *Phys. Rev.* **178** 6105
Raynor G V and Waldrom M B 1949 *Phil. Mag.* B **40** 198
Rooke G A 1968a *J. Phys. C: Solid State Phys.* **1** 767
Rooke G A 1968b *J. Phys. C: Solid State Phys.* **1** 776
Rooke G A 1974 *X-Ray Spectroscopy* ed L V Azaroff (New York: McGraw-Hill)
Sabiryanov R F and Bose S K 1994 *J. Phys.: Condens. Matter* **6** 6197
Sadoc A and Dubois J M 1993 *J. Non-Cryst. Solids* **153–4** 83
Sham T K 1985 *Phys. Rev.* B **31** 1888
Shechtman D, Blech I, Gratias D and Cahn J W 1984 *Phys Rev. Lett* **53** 1951
Stadnik Z M, Purdie D, Garnier M, Baer Y, Tsai A-P, Inoue A, Edagawa K, Takeuchi S and Buschow K H J 1997 *Phys. Rev.* B **55** 10 938
Terakura K 1977 *J. Phys. F: Met. Phys.* **7** 1773
Trambly de Laissardière G, Mayou D and Nguyen Manh D 1993 *Europhys. Lett.* **21** 25
Trambly de Laissardière G, Nguyen Manh D, Magaud L, Julien J P, Cyrot-Lackmann F and Mayou D 1995 *Phys. Rev.* B **52** 7920
Tsai A P 1997 *Mater. Res. Soc. Bull.* **22** 43
von Barth U and Hedin L 1972 *J. Phys. C: Solid State Phys.* **5** 1629
Vuillemin J J and Priestley M G 1965 *Phys. Rev. Lett.* **14** 307
Zhang G W, Stadnik Z, Tsai A P and Inoue A 1994 *Phys. Rev.* B **50** 6996